Design of a passive device for a maximum shadow on roofs in a warm humid climate

Carlos Fernando Arias Martínez, Jenniffer Guadalupe Jiménez Anzar, Carlos Javier Esparza López, Jorge Armando Ojeda Sanchez

Facultad de Arquitectura y Diseño, Universidad de Colima. Km. 9 Ctra.-Coquimatlán, Colima, 28400, Colima, México.

Abstract

Buildings and homes in warm humid climates are major sources of energy consumption, and roofs are generally exposed to the greatest solar gain, leading to overheating. Shading devices are passive solutions that reduce solar irradiance gains. However, the shape of these devices is based on reused materials or fixed geometries, considering aspects such as orientation. In the present work, we analyze the geometric configuration of a shading device that can control the incoming solar gain on roofs by the maximum shading length. The optimal device design is derived from the application of solar geometry and the principles of the constructal design methodology. The shading device's optimal geometric configuration maximizes the shading length in summer and winter in a warm humid climate. The shading device arrangement on the roof of a low-income house was analyzed by numerical simulation for different aspect ratios of the devices, reducing the temperature by an average of 2.2 °C for an aspect ratio of $l_H / l_D = 2$. This configuration offers a 0.5 *kW* reduction compared with the case without shading devices. The shading devices contribute to the set of passive solutions to achieve adequate conditions (energy and habitability) in warm humid climates.

Keywords: shading device, geometry, passive device, shadow length, thermal performance

Introduction

In warm-humid climates, roofing surfaces are critical contributors to internal heat loads, particularly in low-cost dwellings with minimal insulation or thermal mass. Roofs are exposed to high direct solar irradiance for extended periods and thus act as heat conduits into interiors, elevating indoor operative temperatures and intensifying cooling demands. Therefore, passive shading strategies at the roof level are an attractive, low-energy intervention to mitigate these heat gains, reduce reliance on mechanical cooling, and enhance thermal comfort in tropical housing contexts.

Historically, solar control design guidance relied on classical rules of thumb based on solar altitude and azimuth, as codified in works such as Olgyay & Olgyay (Olgyay, 2015). These principles (e.g., overhang depths, projection factors) provide a foundational baseline for shading device sizing. However, over the past decades, the increasing sophistication of building simulation tools has prompted a more rigorous optimization of shading geometries, particularly in facades. Recent envelope frameworks integrate multiple objectives, such as energy consumption, daylighting, visual comfort, and thermal comfort, into unified design tools (Nasrollhzadeh, 2021). However, much of this effort is concentrated on vertical facades rather than roof surfaces. One promising class of hybrid solutions converts roof-mounted modules into photovoltaic (PV) systems that also serve as shading elements. Roof-mounted PV arrays reduce net solar flux on roof membranes, thereby attenuating the upward heat flow into top rooms or attic spaces while simultaneously generating electricity. Nonetheless, these studies often emphasize well-insulated or conditioned buildings in higher-income settings, with less attention to low-cost housing or the geometric optimization of PV arrays purely as shading devices (Albatayneh 2022; Ma 2023; Shen 2022).

The dual nature of such systems introduces coupling between thermal shading performance and PV efficiency, since elevated PV temperatures may degrade electrical

Dates
Received: December 20, 2025
Accepted: March 12, 2026
Available online: April 2026

Corresponding author
Jorge Armando Ojeda Sánchez
jojeda1@ucol.mx
ORCID: https://orcid.org/0000-0002-5026-5459

Cite this article
Arias Martínez CF, Jiménez Anzar JG, Esparza López CJ, Ojeda Sánchez JA (2026). Design of a passive device for a maximum shadow on roofs in a warm humid climate. *Ciencia Nicolaita* 96:100-112. DOI:10.35830/cn.vi96.898

output, thereby complicating optimal trade-offs. Parametric and multi-objective optimization methods have been applied to the design of overhangs, fins, louvers, and adaptive shading systems in parallel to hybrid shading. For example, global optimization algorithms and sensitivity analysis are used to identify the parameters (depth, angle, and spacing) that dominate thermal and daylight outcomes in light-shelf and façade shading. These tools have sharpened our understanding of the trade-offs between daylighting quality and solar gain control (Bahdad,2021). Importantly, while these techniques are well developed for façades, their adaptation to roof-mounted passive geometries (e.g., flat overhangs, double plates, tilt angles) remains underexplored. Several case-based and simulation studies have been conducted in the hot-climate domain of roof-level shading. Some studies have examined fixed overhang optimization for residential buildings and found modest but measurable cooling demand reductions (e.g., 4% in a study in Casablanca) (Sghiouri, 2018). Others have analyzed the shading performance of rooftop configurations in particular climate zones, exploring trade-offs in plate orientation or shading depth (García,2020). However, many such studies adopt climate contexts outside truly humid-tropical conditions or do not systematically optimize device geometry across seasonal extremes.

Recent research has extended the investigation of shading devices to region-specific climates. For instance, the performance of artificial shading devices in Saudi contexts was evaluated under different materials (Tahir, 2025). The cooling effect of fixed external shading devices in hot-humid cities was assessed, but mostly from a material or orientation standpoint rather than full parametric optimization (Homod,2021). In the literature on building envelope, the coupling of thermal comfort, daylighting, and energy performance for façade and roof elements was explored in hot climates, showing energy savings up to 25% when design variables like window-to-wall ratio and shading dimensions are jointly optimized (Wu 2025; Yang 2025). Despite these advances, the literature exhibits recurring gaps and limitations:

1. Lack of geometric optimization specifically for roof-mounted passive shading devices: While shading on facades is well studied, the roof as a plane requiring seasonal solar protection under tropical sun angles is far less explored with constructal or analytic design methods.

2. Scant focus on low-cost or mass-produced housing contexts: Many studies assume high-spec envelope assemblies, active cooling, or complex installations that are impractical for low-income housing. Limited works are tailored for simple construction constraints, economic viability, and ease of installation.

3. Insufficient integration of field calibration and simulation: Many proposals remain in simulation-only form; shading designs in vernacular homes are validated via monitored field data and dynamic model calibration.

4. Limited exploration of trade-offs among shading depth, tilt, spacing, and orientation under humid-tropical solar regimes across seasons. Only a few studies have traversed both summer and transitional seasons with optimized configurations.

5. Underexplored coupling between shading effectiveness and PV performance for roof-mounted arrays functioning concurrently as shading devices, especially in contexts where PV temperature sensitivity and shading geometry strongly interplay.

Given these gaps, this paper seeks to contribute by systematically analyzing a two-plate passive shading device with maximum shadow length. Designed for roof applications in warm-humid climates, focusing on low-cost implementation. The shading device size and geometric configuration were determined using well-known solar geometry and solar height expressions. Any geometric configuration on any other date and its respective solar altitude is included between the two solar altitudes that correspond to the summer and winter solstices. The device design does not consider the cumulative irradiances from the sun and the sky as a barrier. Specifically, the work: (i) formulates analytic geometric relationships (plate lengths, tilt angles, and spacing) to maximize shading over critical solar angles within constructal method (Miguel, 2008); (ii) couples these geometric designs with calibrated dynamic simulations (via EnergyPlus/Design Builder software) applied to representative mass-produced housing units; and (iii) evaluates the thermal performance (operative temperature reduction, cooling load impact) of optimized versus baseline configurations. Thus, this research bridges analytic geometry, pragmatic constraining, and simulation validation to address a knowledge gap in roof shading for tropical housing design and retrofit.

Methodology

This work was developed in different stages. Initially, the study site's climatic characteristics were presented, fol-

lowed by the identification of a case study for shading device analysis. A low-cost, low-income housing unit was selected. Subsequently, expressions defining the shading device's geometric configuration were developed. The angles and the relationship between the lengths of the panels that provide the maximum shading length were identified on two representative dates: summer and winter solstice. In addition to recording the temperature, humidity, and outdoor radiation, temperature and humidity measurements are made in a low-income house. The obtained data were used to calibrate the simulation model. Finally, once the simulation model was calibrated, a simulation analysis was conducted for different geometric configurations of the shading device, applied to the roof of a low-income house, and its effect on indoor temperature, as a first approximation to the application of the constructal methodology to architectural elements. The methodology is illustrated in **Figure 1**.

Climatic conditions

The present work was conducted in Colima, México at 19°14'40" N, 103°46'28" W, and 484 m above sea level, which has a hot humid climate characterized by elevated temperatures and high levels of humidity. The average annual temperature is 26.4 °C, thermal swing is 14.7 °C with an annual rainfall is 856.3 mm (SMN, 2010). According to the Köppen-Geiger classification, the climate is an equatorial savanna climate with a dry winter (Aw) (Kottek, 2006). **Figure 2** shows a map of the study area geographically referenced with latitude and longitude markings.

In **Figure 3**, shows the maximum, mean, and minimum dry bulb temperature (DBT) and relative humidity (RH), where the three main climatic seasons can be observed. The warm subhumid season occurs from January to March and November to December, with a mean temperature of 24.5 °C and a RH of 60.9%. The hot sub-humid season runs from April to May with mean values of temperature and RH of 26.2 °C and 63%, respectively. Finally, the hot humid season, which runs from June to November, has an average temperature and RH of 27.3 °C and 73%.

To evaluate shading devices, low-income, mass-built houses in urban developments must first be identified. This type of housing was developed to meet the needs of the population of Colima, Mexico. These 104 m^2 houses comprised two bedrooms, a bathroom, a kitchen, and a dining room. Social housing conditions in warm climates often fail to provide adequate habitability conditions due to the inherent challenges associated with these environments. The high temperatures and humidity levels in these climates can lead to a range of issues, including heat stress, moisture damage. Residents of these areas frequently experience discomfort and health problems (Flores, 2021).

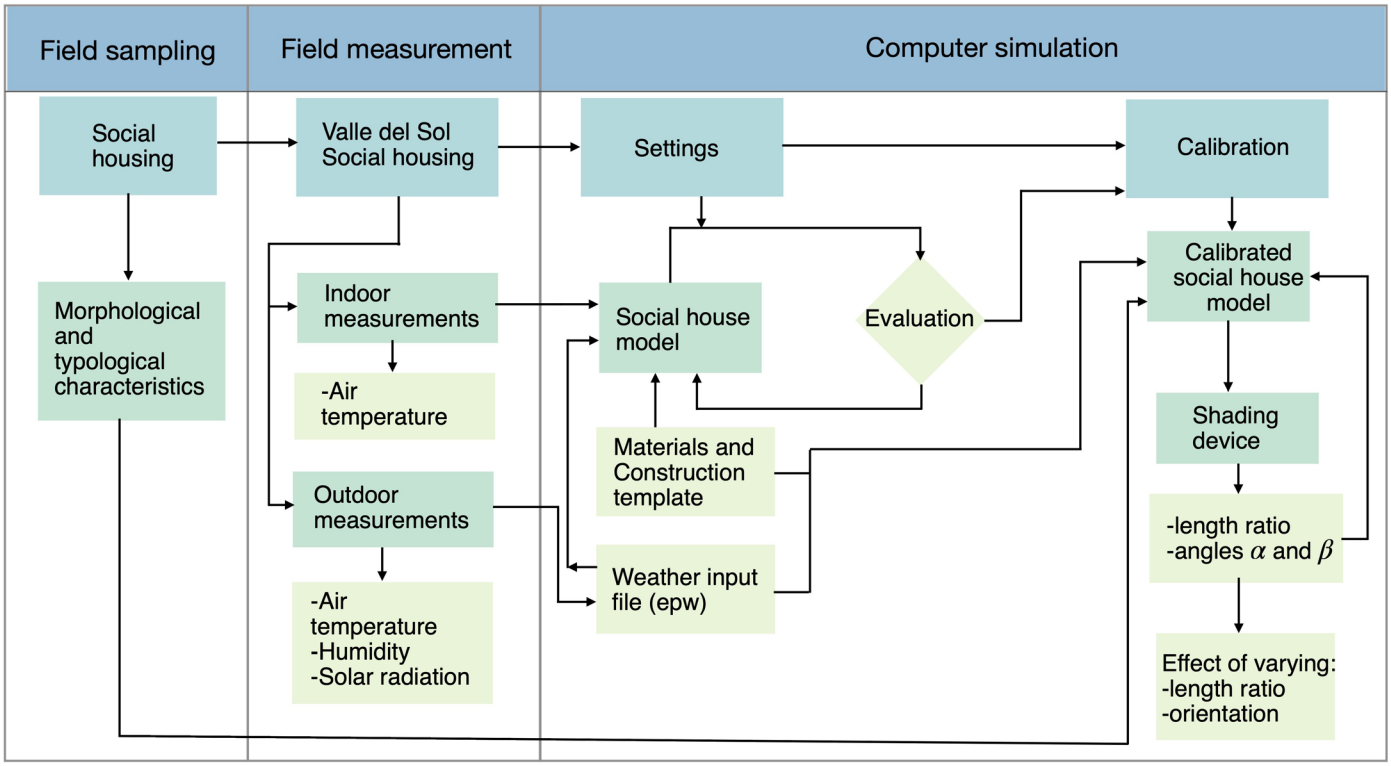

Figure 1. Flowchart of the methodology.

Figure 2. Study area in Colima, Mexico (INEGI, 2026; OpenStreetMaps, 2026).

The selected house is located in a low-income house development *Valle del Sol*, in the municipality of Villa de Álvarez, Colima, Mexico, at approximate coordinates 19°14'40" N, 103°46'28" W, and 484 m above sea level. Indoor conditions, such as dry bulb temperature and relative humidity, were recorded using OnsetComp data loggers with an accuracy of ±0.35 °C. Outdoor conditions, such as dry-bulb temperature, humidity, and solar radiation, were recorded by the weather microstation, model H21-0021.

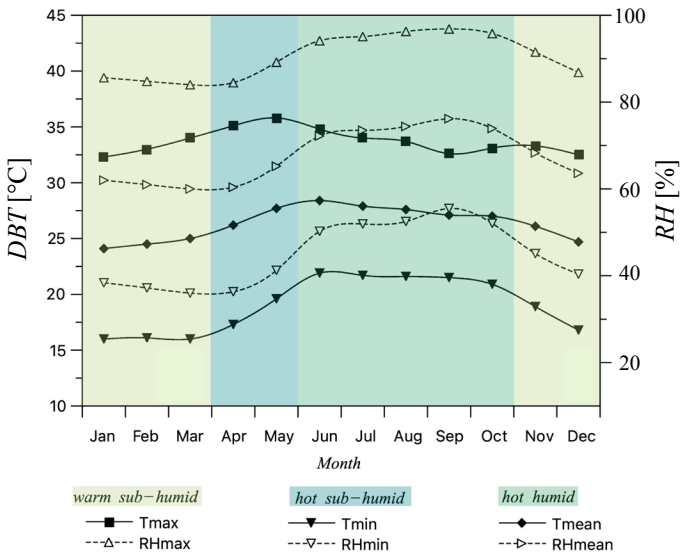

Figure 3. Dry bulb temperature and relative humidity for Colima, México.

The measurement period was from October 13th to 22th, 2022. In **Figure 4**, shows the house configuration and distribution of the measuring instruments. The measurements above helped us generate a weather file (epw), which is necessary for computer simulation.

Shading device design

To define the geometry of the shading device such that it projects the maximum shading length on the roof in two main climatic seasons in a hot humid climate, the shading device comprises two plates of thickness e and width w with lengths l_H and l_D. One of the plates is inclined at an angle α, the second plate is arranged at an angle β, which, for shading purposes, is considered with a value $\beta \leq 90°$, for simplicity, the width w is considered constant. A sketch of the proposed device is shown in **Figure 5**. The main requirements are the maximization of shading length and plate size.

To determine the maximum shading length of the device, the angles α and β, which are unknown, were considered in addition to the solar height h. The solar heights corresponding to the summer and winter solstices, defined below, are used for the Coquimatlán latitude. The law of sine can be used to obtain the relationship between the shading length, plate length, and angles necessary to obtain maximum shading. The relationships between lengths are defined as follows:

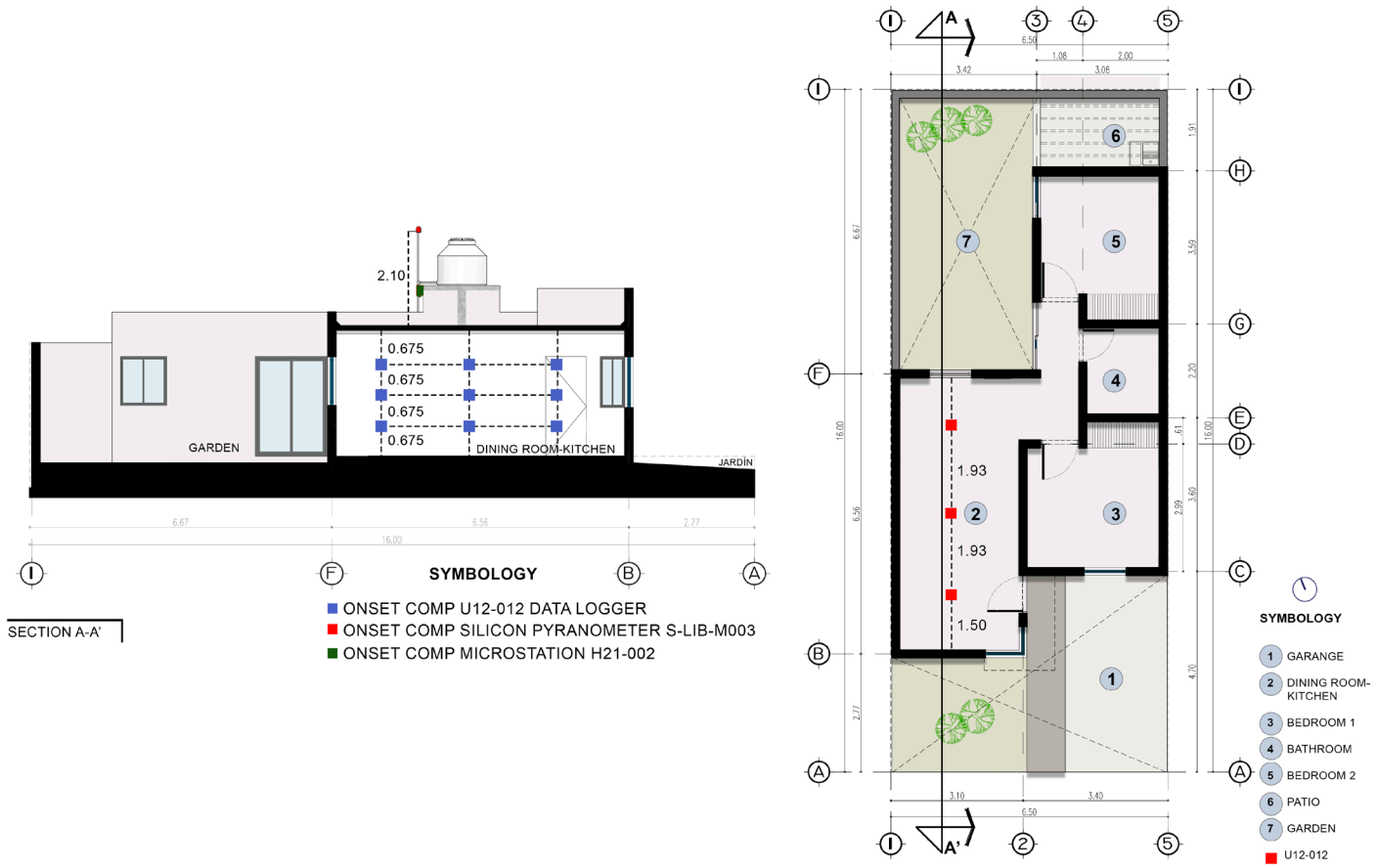

Figure 4. Low-income house at Valle del Sol, Colima, Mexico. **a)** House layout with measurement instruments, section A- A'. **b)** Floor plan.

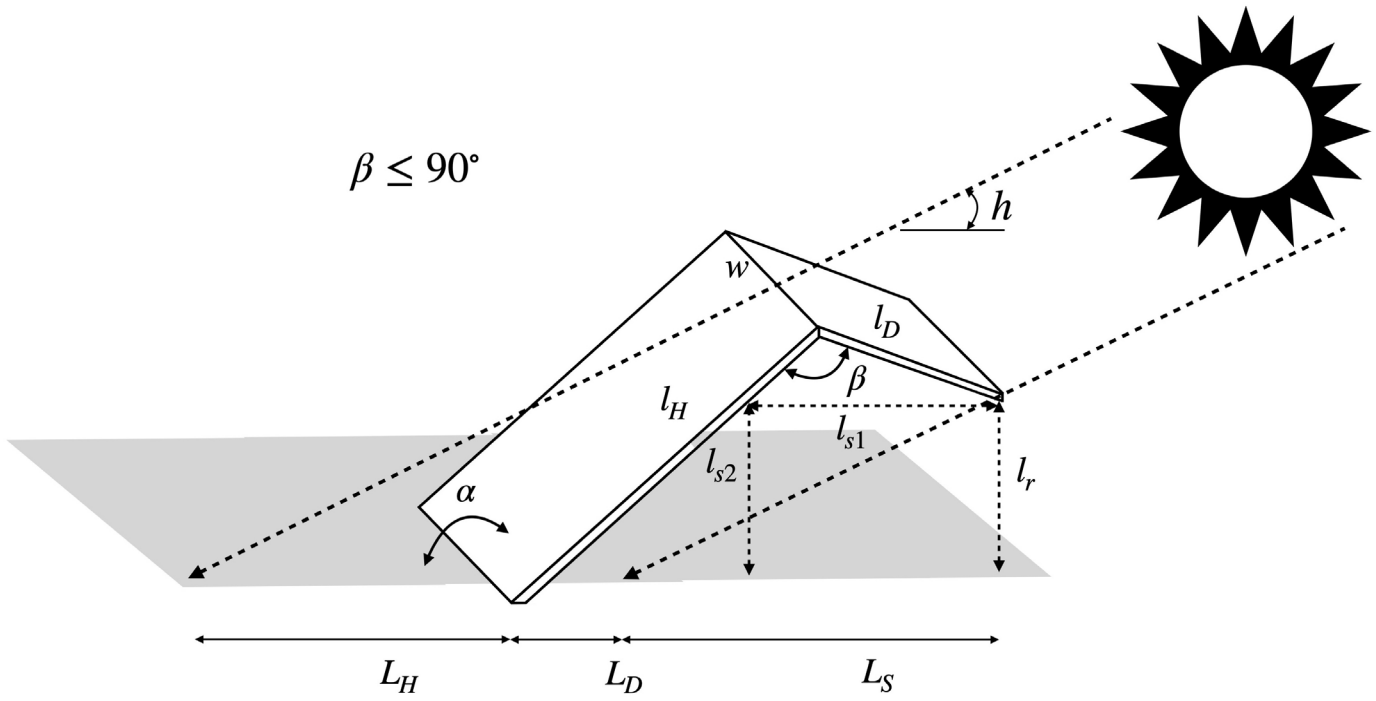

Figure 5. Schematic diagram of the shading device, based on the work of Miguel, 2008.

$$\frac{\sin(h)}{l_H}=\frac{\sin(\alpha+h)}{L_H}, \tag{1}$$

$$\frac{\sin(180-\alpha)}{l_r}=\frac{\sin(\alpha-90)}{l_{s1}}, \tag{2}$$

$$\frac{\sin(\beta)}{l_{s2}}=\frac{\sin(180-\alpha)}{l_D}, \tag{3}$$

$$\frac{\sin(h)}{l_r}=\frac{\sin(90-h)}{L_s}, \tag{4}$$

and

$$L_D=l_{s1}+l_{s2}-L_s. \tag{5}$$

Where h is the solar height h, l_{s1}, l_{s2}, l_r, and l_s are the lengths of the shading device, and L_H and L_D are the shading lengths projected by the plates of length l_H and l_D, respectively, as shown in **Figure 5**. From **Eqs. (1) - (5)**, the following length relations can be easily obtained:

$$\frac{L_H}{l_H}=\sin(\alpha)\cot(h)+\cos(\alpha), \tag{6}$$

$$\frac{L_D}{l_D}=\frac{\sin(\beta)}{\sin(\alpha)}-\left(\frac{l_H}{l_D}\sin(\alpha)-\sin(\alpha-\beta)\right)\left(\cot(\alpha)-\cot(h)\right). \tag{7}$$

Eqs. (6) and (7) show the relationship between the shading length and the plate length in terms of the plate inclination angles and the solar height h. On the other hand, **Eq. (7)** is expressed in terms of the length ratio l_H / l_D, which is considered a parameter for determining the inclination angles and maximum shading lengths of each plate. A constraint must be defined to maximize the shading length, where the length ratio is considered constant, $l_H+l_D = constant$.

To determine the solar height h, the solar declination β and solar azimuth α were determined by the well-known equations of solar geometry (Wald, 2021). These expressions are given by:

$$h=\arcsin\left(\begin{matrix}\sin(\phi)\sin(\beta)+\\ \cos(\phi)\cos(\beta)\cos(z)\end{matrix}\right), \tag{8}$$

$$a=\arcsin\left(\cos(\beta)\sin(z)/\cos(h)\right), \tag{9}$$

$$\beta=\arcsin\left(0.398\sin\left(0.9863(d-82)\right)\right), \tag{10}$$

where z is the solar elevation, given by $z = 15(t - 2)$, ϕ, t, and d are the latitude, solar hour, and the Julian day, respectively.

The solar height h during the summer and winter solstices was considered for the latitude of Colima. These events occurred on June 21 ($d = 172$) and December 21 ($d = 355$) around the solar midday ($\pm 2h$), which is when the greatest thermal loads on roofs occur due to solar exposure, as a first approximation to the problem. The corresponding solar heights for the summer and winter solstice are $h_1 = 1.339$ and $h_2 = 0.791$, respectively. The shading device's geometric characteristics were evaluated considering these two solar heights. For this work, the length ratios $l_H/l_D = 0.5$, 1, and 2 were used, with the corresponding values of the angles α and β, for each solar height. Appendix A provides details on the geometric arrangement and angles of the plates for different l_H/l_D values.

Table 1. Geometrical characteristics of the shading device.

Case	l_H [m]	l_D [m]	l_H/l_D	$\alpha(h_1)$ [°]	$\alpha(h_2)$ [°]	β [°]
I	0.5	1	0.5	72	103	90
II	0.25	0.5	0.5			
III	0.5	0.5	1	90	122	90
IV	1	1	1			
V	0.5	0.25	2	109	140	90
VI	1	0.5	2			

Calibration

The aforementioned low-income house model must be calibrated for shading device analysis. Analysis was performed using the Design Builder software with Energy Plus as the computational engine for simulating energy performance. The required weather file (epw file) was generated using the Meteonorm software. The measured outdoor data were implemented in the weather file; thus, calibration was performed between October 15th and 21st, 2022. Thus, the indoor dry bulb temperature results were

Table 2. Materials properties used in construction template.

Materials	thickness [m]	density [kg/m^3]	specific heat [J/kgK]	thermal conductivity [W/mK]	R-value [m^2K/W]
walls					0.976
polystyrene	0.025	16	1200	0.04	
brick	0.14	1920	790	0.9	
cement sand render	0.025	1800	1000	1	
roofs					1.536
concrete	0.1	2300	880	1.4	
polystyrene	0.05	16	1200	0.04	
gypsum plastering	0.03	1000	1000	0.4	
floors					0.374
cast concrete	0.01	2000	1000	1.13	
ceramic porcelain	0.02	2300	840	1.3	
windows					0.261
single clear	0.003	-	-	0.9	
aluminum frame	0.05	2800	880	160	

compared with those obtained using the simulation program.

In order to perform the simulation necessary for comparison with the measured data, a template for the construction system of mass-produced low-income houses was generated. A block system was used for the exterior and interior walls. The exterior walls contained a polystyrene slab that acted as insulation for the adjacent walls. The roof was made of concrete, polystyrene slab, and gypsum plaster. The materials used in the Design Builder construction template, including their physical properties. The material properties are listed in **Table 2**.

To validate the simulation model, two data sets of hourly calculated and measured indoor dry-bulb temperatures were compared. The simulated temperature data were compared using the average indoor operative air temperature, which was recorded by the common kitchen and dining area data loggers, as the observed variable. The model performance was determined by the calculation of the mean absolute error percentage (MAPE) (Chicco, 2021), which leads to the calculation of the mean absolute relative error percentage (PMARE), yielding values 2.28%. According to Ali (2021), the percentage value obtained was rated as excellent.

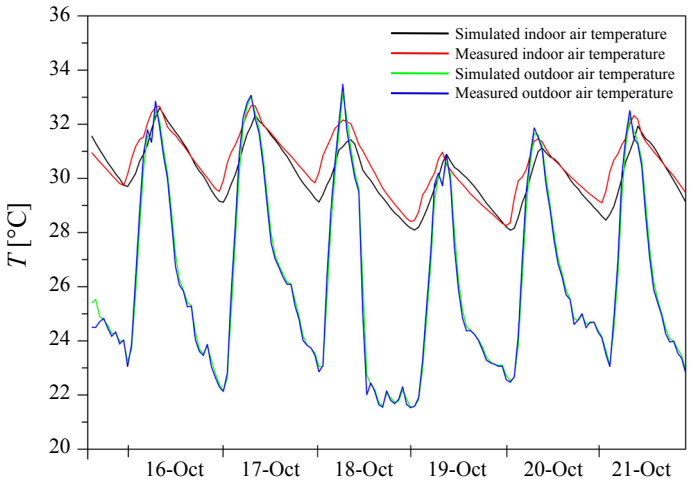

Figure 6. Comparison of measured and simulated air temperature.

Simulation scenarios

To assess the impact of roof-mounted shading devices on low-income social housing, we identified representative days for each climatic season. A representative day (RD) is one on which the temperature and relative humidity conditions are most similar to the climatic season. A representative day is one in which the sum of the two differences—between the average daily and seasonal temperatures and the daily and seasonal thermal swing is close to zero (Esparza, 2022). The representative day is given by the following empirical expression:

$$RD = \left| T_{avg_{daily}} - T_{avg_{season}} \right| + \left| TS_{avg_{daily}} - TS_{avg_{season}} \right| \approx 0. \quad (11)$$

The daily average temperature and thermal swing for each climatic season were calculated using the epw climate file data as $T_{avg_{daily}}$ and $TS_{avg_{daily}} = T_{max} - T_{min}$. The data

Table 3. Representative days for climatic season.

Climatic season	$T_{avg_{daily}}$ [°C]	$TS_{avg_{daily}}$ [°C]	$T_{avg_{season}}$ [°C]	$TS_{avg_{season}}$ [°C]	RD
Warm sub-humid	25.27	10.91	24.88	11.3	January 19th
Hot sub-humid	26.05	19.7	27.1	13.05	April 9th
Hot humid	27.62	6.79	26.07	8.34	June 28th

required to determine the climatic seasons were defined from the meteorological database of the National Water Commission of Mexico . In **Table 3** the representative day data for each climatic season required to determine the representative days for each season.

The effect of the shading device on the indoor temperature of the house will be analyzed on the aforementioned representative days. The geometric configuration of the shading device depends on the aspect ratio l_H / l_D and the solar heights.

Results

This section presents the simulation results of the indoor operating temperature of the different shading devices on the roof of a low-income housing unit. The results are presented for the three climatic seasons for a shading device with fixed aspect ratios l_H / l_D = 0.5, 1 and 2, for the summer and winter solstice solar heights, h_1 and h_2, values that determine the angles of each shading device panel. The shading devices were modeled in Design Builder and arranged in an east-west orientation, so that the shadow of one device is projected onto the initial portion of the next, thus avoiding solar gain on the roof surface of the low-income housing unit. In practice, roofs typically house essential elements such as water tanks, solar water heaters. Considering these elements along with shading devices would require the modification of the shading device distribution in a modular arrangement to allow for walkability and access. These roof elements are omitted as a first approximation to evaluate the reduction of solar heat gain through shading. Unlike solar collectors or photovoltaic panels, which must be oriented to the south, with an angle of inclination according to the site's azimuth, to receive sunlight for as long as possible. The simulation model in Design Builder considers neighboring houses, represented as component blocks, without necessarily containing thermal zones. The house was modeled using the corresponding material templates, with materials used in the validation stage are shown in **Table 1**. **Figure 7** shows the design builder model of a low-income house with shading devices, with a ratio l_H / l_D = 2 and an East-West orientation.

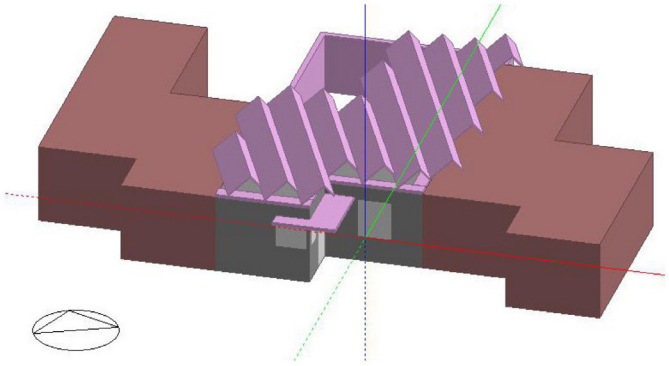

Figure 7. Design Builder model for the low-income social housing with a shading device with l_H / l_D = 2.

The simulation results correspond to the indoor operating temperatures of the kitchen-dining room, in the unshaded case, T_{base}, and of the shading devices, which correspond to solar heights h_1 and h_2. For clarity, the results are shown with double axes to appreciate the reduction in indoor temperature relative to the outdoor temperature, where the right axis corresponds to the representative day of the outdoor temperature for each climatic station. **Figure 8** shows the indoor temperatures for the representative day of January 19th, during the warm sub-humid season for different l_H / l_D values.

The warm sub-humid season, which includes November to March, represents the mildest season of the year, with average temperatures and relative humidity of 25 °C and 60%. The maximum outdoor temperature on the representative day is $T_{outdoor}$ = 31 °C and occurs at 16:00. The indoor temperature for the case of the home without a shading device occurs at 18:00, with a temperature reduction with respect to the outside of 2.1 °C. In **Figure 8a** shows the effect of shading devices on the indoor temperature for a length ratio l_H / l_D = 0.5. The indoor temperatures $T_{II\text{-}h1}$ and $T_{I\text{-}h2}$ slightly differences. The indoor temperature $T_{I\text{-}h2}$, which corresponds to case I, of the **table 1** with the angles corresponding to the solar height h_2, presents a slightly greater reduction in indoor temperature than the maximum exterior temperature. The maximum indoor temperature reduction due to the shading device with respect to the outdoor temperature is 2.54 °C and 2.62 °C, respectively. The thermal delay of these temperatures occurs at the same time as T_{base}.

The indoor temperatures, corresponding to the shading devices defined by the length ratios l_H / l_D = 1 and 2 are shown in **Figure 8b** and **c**. For a length ratio l_H / l_D =

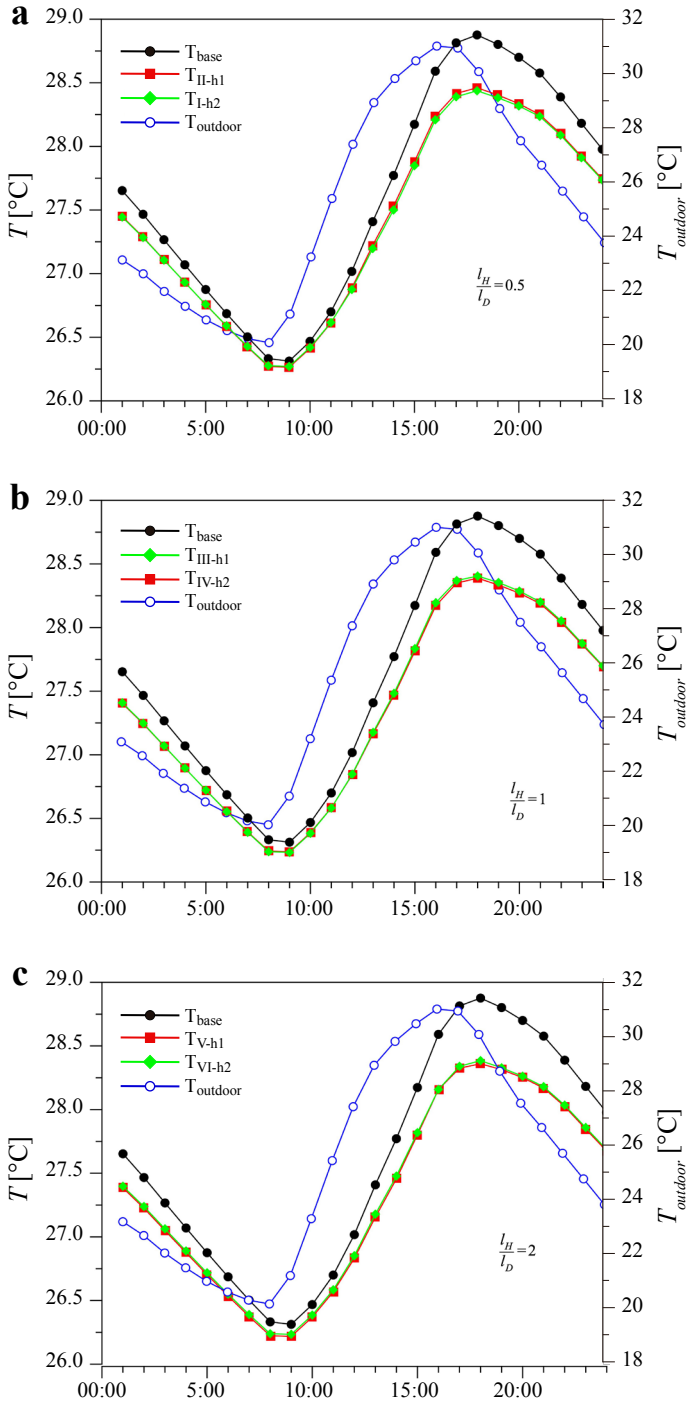

Figure 8. Comparison of temperatures versus time for the shading device for solar heights h_1 and h_2 for **a)** $l_H / l_D = 0.5$, **b)** $l_H / l_D = 1$ and **c)** $l_H / l_D = 2$ in the representative day for the warm sub-humid season.

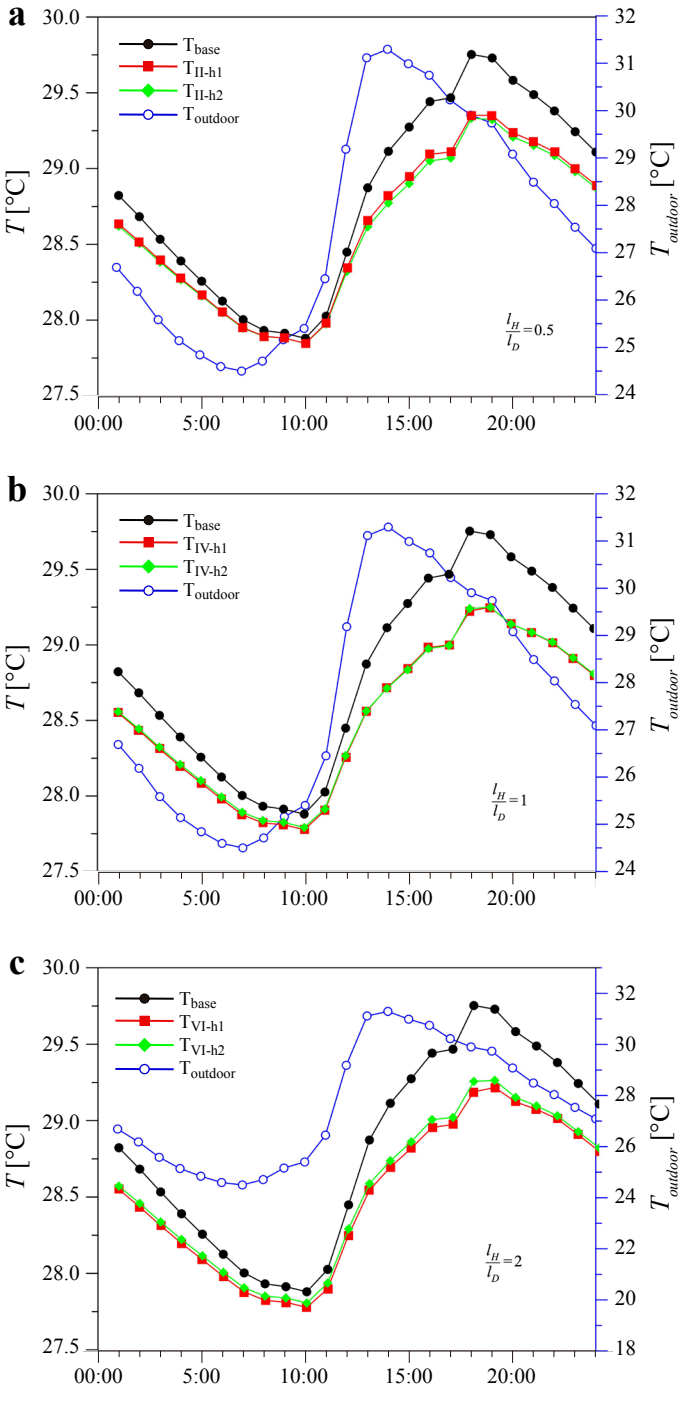

Figure 9. Indoor temperatures with the shading device for different aspect ratios l_H / l_D at a solar height h_1 in the hot sub-humid season.

1, the maximum interior temperatures of T_{h1} and T_{h2} show temperature reductions of the order of 25 °C, representing 0.5 °C more than the maximum value of T_{base}. Conversely, for a device with a length relationship $l_h / l_D = 2$, a reduction in indoor temperature of 2.6 °C is observed with respect to the maximum outdoor temperature value.

The hot sub-humid season is characterized by average temperatures of 27 °C, maximum values of 35 °C and an average relative humidity percentage above 90%, which can cause a higher thermal sensation indoors. The shading device with the length ratio $l_H / l_D = 0.5$ presents a smaller decrease in interior temperature than in the previous climatic season. The simulated indoor temperature T_{base}, presents a maximum indoor temperature similar to the outdoor temperature with a temperature difference of

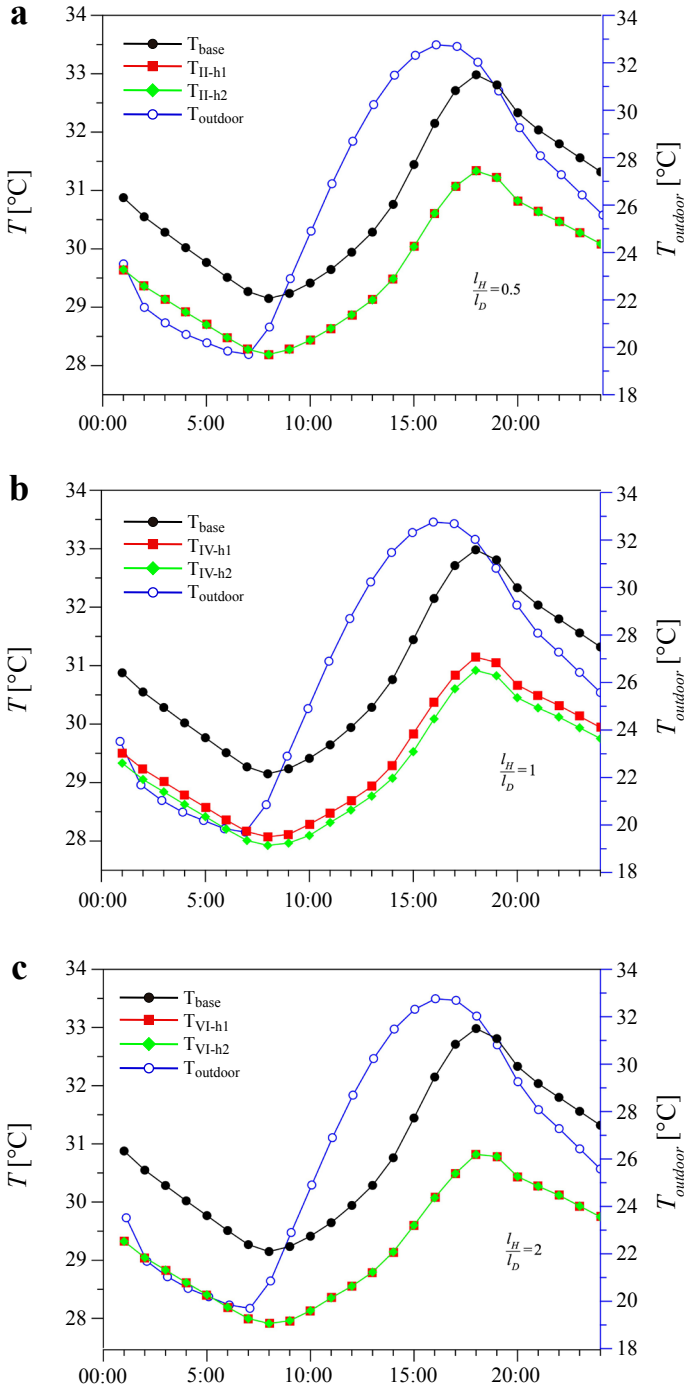

Figure 10. Comparison of temperatures versus time for the shading device for solar heights h_1 and h_2 for **a)** $l_H / l_D = 0.5$, **b)** $l_H / l_D = 1$ and **c)** $l_H / l_D = 2$ in the representative day for the hot humid season.

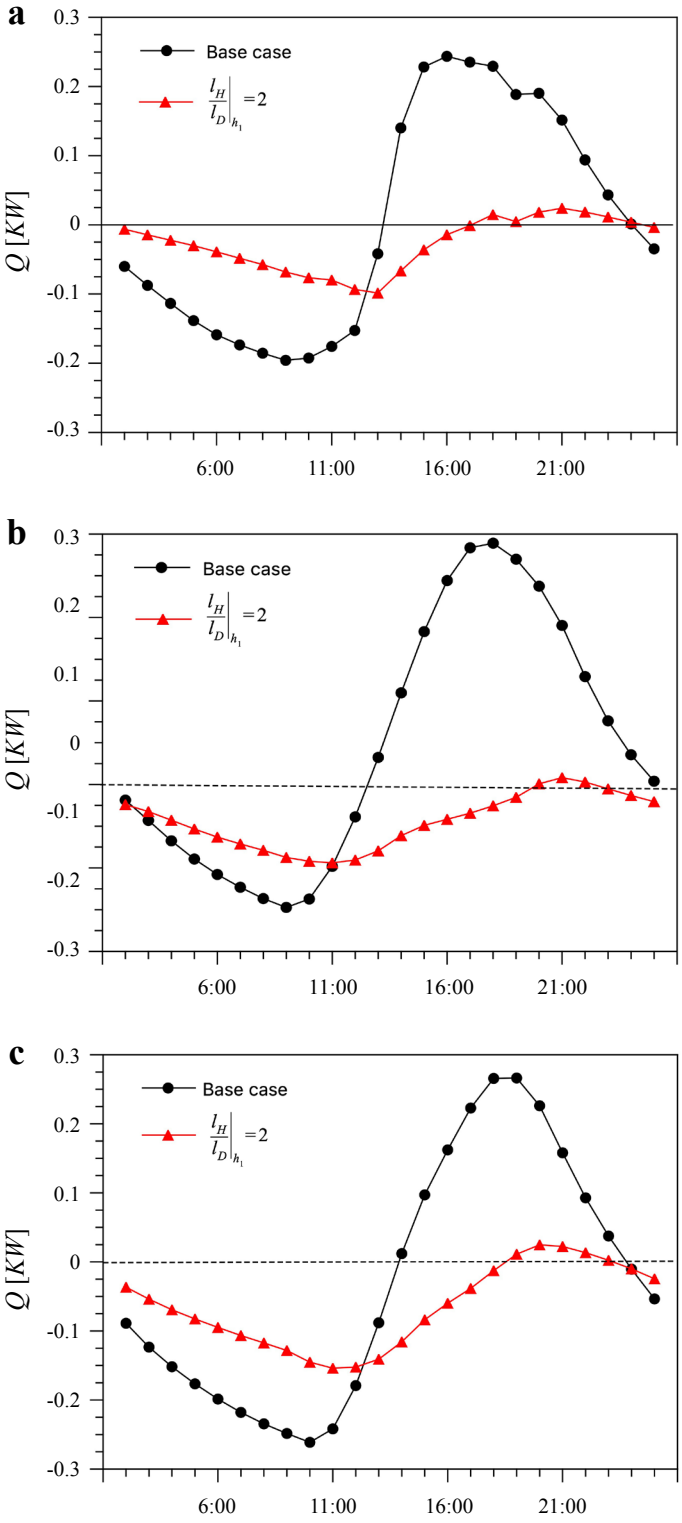

Figure 11. Comparison of the heat gains in roofs for the base case versus shading device with $l_H / l_D = 1$ for **a)** warm sub humid season, **b)** hot sub humid season **c)** hot humid season.

1.9 °C and a thermal delay of 2 hours. This feature can be observed in **Figure 9a**.

For a shading device with a length ratio of l_H / l_D = 1, in **Figure 9b** shows that the indoor temperatures $T_{IV\text{-}h1}$ and $T_{IV\text{-}h2}$, show an approximately temperature reduction with respect $T_{outdoor}$ of the order of 2 °C. Conversely, for the device with a length ratio l_H / l_D = 2, a reduction in maximum interior temperatures, relative to the maximum value of $T_{outdoor}$, of 1.9 and 2.0 °C respectively. This can be seen in **Figure 9c**. The warm humid season presents high humidity conditions and high dry bulb temperature,

with average maximum temperatures of 27 °C and 35 °C and maximum RH above 90%. For the case without shadowing protection, the thermal delay between the maximum outdoor and indoor temperatures was 4 h, and the maximum temperature reduction with respect to $T_{outdoor}$ value was 2.0 °C. **Figure 10a** shows that the reduction in the maximum indoor temperature due to the shading device with a ratio $l_H / l_D = 0.5$ is of the order of 1.4 °C. For the following length ratios, which are depicted in **Figures 10b** and **c**, the reduction in indoor temperature for a device with $l_H / l_D = 1$, the maximum temperature reduction with respect to the maximum outdoor temperature value was $T_{IV\text{-}h1} = 1.6$ and $T_{IV\text{-}h2} = 1.8$ °C. However, for a shading device with a ratio $l_H / l_D = 2$, the maximum temperature reduction is 1.9 °C, for the devices given by h_1 and h_2.

The thermal gains due to the different shading device configurations show that the shape configuration with the lowest energy gain to the interior space is given by a length ratio $l_H / l_D = 2 (l_H = 0.5, l_D = 0.25)$ for a solar height h_1. In **Figure 11**, the base case heat gains without shading protection versus the heat gain from the shading device for each climate season. The greatest reduction in heat gains Q [KW], of approximately 0.51 [KW] occurs in the warm sub-humid season. However, for the hot sub-humid and hot humid seasons, the reduction is 0.24 and 0.22 [KW], respectively. Positive and negative values denote heat gains into and losses from the space.

Conclusions

In this work, the concepts of solar geometry and design principles of the constructive method were applied to determine the design of a passive shading device on the roof of a low-income house in a warm sub-humid climate. The shading device with the greatest indoor temperature reduction was for a radius of lengths $l_H / l_D = 2$ for corresponding summer and winter solar heights. In a warm sub-humid climate, the implementation of passive strategies is a first strategy to adapt a building to climatic variations of high temperatures and relative humidity, in such a way that the shading device is a first approach to the application of the constructive method, to analyze the form and structure, which satisfies a global objective, *i.e.* maximum shading length, subject to local restrictions. The obtained geometries reduce the indoor temperature while avoiding thermal gains in the roof and its consequent transfer to the interior. This design methodology was developed for climates with a wide range of seasonal temperature variations. The results are a first approach to developing passive solutions that complement active systems in warm climates.

Acknowledgements

The authors acknowledge the support of the Secretaría de Ciencia, Humanidades, Tecnología e Innovación (SECIHTI) for postgraduate scholarships for C. Arias and J. Jiménez-Anzar.

Disclosure statement

The authors declare that they have no known competing financial interests or personal relationships that could have appeared to influence the work reported in this paper.

Availability of data

The data that support the findings of this study are available from the corresponding author upon reasonable request.

Author contributions

Conceptualization, J.A.O., C.A.; methodology, J.A.O. and C.A.; formal analysis, J.A.O., C.A., J.J.; writing—original draft preparation, J.A.O. and C.E.; writing—review and editing, J.A.O and C.E. All authors have read and agreed to the published version of the manuscript.

References

Albatayneh A, Albadaineh R, Juaidi A, Abdallah R, Montoya MDG, Manzano-Agugliaro F (2022). Rooftop photovoltaic system as a shading device for uninsulated buildings. *Energy Reports* 8:4223-4232. doi:10.1016/j.egyr.2022.03.082.

Ali MH, Abustan I (2021). A new novel index for evaluating model performance. *JNRD - Journal of Natural Resources and Development* 4:1-9. doi:10.5027/jnrd.v4i0.01.

Bahdad AAS, Fadzil SFS, Onubi HO, BenLasod SA (2021). Sensitivity analysis linked to multi-objective optimization for adjustments of light-shelves design parameters in response to visual comfort and thermal energy performance. *Journal of Building Engineering* 44:102996. doi:10.1016/j.jobe.2021.102996.

Chicco D, Warrens MJ, Jurman G (2021). The coefficient of determination R-squared is more informative than SMAPE, MAE, MAPE, MSE and RMSE in regression analysis evaluation. *PeerJ Computer Science* 7. doi:10.7717/peerj-cs.623

Esparza-López CJ, Pozo CE, Al-Obaidi KM, González-Trevizo ME (2022). Improving the thermal performance of indirect evaporative cooling by using a wet fabric device on a concrete roof in hot and hu-

mid climates. *Energies* 15:6. doi:10.3390/en15062213.

Flores-Larsen S, Filippín C (2021). Energy efficiency, thermal resilience, and health during extreme heat events in low-income housing in Argentina. *Energy and Buildings* 231:110576. doi:10.1016/j.enbuild.2020.110576.

García-Solórzano LA, Esparza-López CJ, Al-Obaidi KM (2020). Environmental design solutions for existing concrete flat roofs in low-cost housing to improve passive cooling in western Mexico. *Journal of Cleaner Production* 277:123992. doi:10.1016/j.jclepro.2020.123992.

Homod RZ, Almusaed A, Almssad A, Jaafar MK, Goodarzi M, Sahari KSM (2021). Effect of different building envelope materials on thermal comfort and air-conditioning energy savings: A case study in Basra city, Iraq. *Journal of Energy Storage* 34:101975. doi:10.1016/j.est.2020.101975.

INEGI (2026). *Cuéntame de México*. https://cuentame.inegi.org.mx/imprime_tu_mapa/

Kottek M, Grieser J, Beck C, Rudolf B, Rubel F (2006). World Map of the Köppen-Geiger climate classification updated. *Meteorologische Zeitschrift* 15(3):259–263. doi:10.1127/0941-2948/2006/0130.

Ma Z, Hu L, Mao H, Shao Q, Tian Z, Luo Y, Deng J, Sun D, Fan J (2023). Shading effect and energy-saving potential of rooftop photovoltaic on the top-floor room. *Solar Energy* 265:112099. doi:10.1016/j.solener.2023.112099.

Miguel AF (2008). Constructal design of solar energy-based systems for buildings. *Energy and Buildings* 40(6):1020–1030. doi:10.1016/j.enbuild.2007.08.005.

Nasrollahzadeh N (2021). Comprehensive building envelope optimization: Improving energy, daylight, and thermal comfort performance of the dwelling unit. *Journal of Building Engineering* 44:103418. doi:10.1016/j.jobe.2021.103418.

Olgyay V, Olgyay A, Lyndon D, Reynolds J, Yeang K (2015). Design with Climate: Bioclimatic Approach to Architectural Regionalism - New and expanded Edition. Princeton University Press. Accessed: 13 October 2025.

OpenStreetMap. (2026). *OpenStreetMap*. https://www.openstreetmap.org/#map=13/19.25289/-103.71780&layers=V

Servicio Metereológico Nacional (2010). Normales Climatológicas. URL:https://smn.conagua.gob.mx/es/climatologia/informacion-climatologica/normales-climatologicas-por-estado?estado=col. Accessed: 4 October 2024.

Sghiouri H, Mezrhab A, Karkri M, Naji H (2018). Shading devices optimization to enhance thermal comfort and energy performance of a residential building in Morocco. *Journal of Building Engineering* 18:292–302. doi:10.1016/j.jobe.2018.03.018.

Shen L, Li H, Guo L, He B-J (2022). Thermal and energy benefits of rooftop photovoltaic panels in a semi-arid city during an extreme heatwave event. *Energy and Buildings* 275:112490. doi:10.1016/j.enbuild.2022.112490.

Tahir IA, Fattah AAE, Mohammed M, Asif M, Almahdy O (2025). Evaluating the performance of outdoor shading devices on human thermal comfort in hot humid climates: A case study of Dhahran. *Building and Environment* 271:112625. doi:10.1016/j.buildenv.2025.112625.

Wald L (2021). Fundamentals of solar radiation. CRC Press / Taylor Francis Group. doi:10.1201/9781003155454.

Wu Z, Xu Y, Wang Z (2025). Multi-objective optimization of energy, view, daylight and thermal comfort for building's fenestration and shading system in hot-humid climates. *PLoS One* 20:e0325290. doi:10.1371/journal.pone.0325290.

Yang F, Zhou H, Chen J, Sun Y, Wang D, Sun F, Zhang L (2025). Energy-Saving Performance and Optimization Study of Adaptive Shading System—A Case Study. *Buildings* 15(11). doi:10.3390/buildings15111961.

Appendix A

Geometric characteristics of the shading device

The geometric characteristics of the shading device are analyzed for different length ratios of each plate, optimal angle, and summer and winter solar heights. Using **Eqs. (6)** and **(7)**, the length relationships L_H/l_h and L_D/l_D of the plates to their shading lengths are analyzed for different values of the angles α and β.

In **Figure A1**, it can be seen that for the ratio L_H/l_h, considering the solar height for the winter solstice, a greater relationship between the shading length and plate length l_H is obtained for the winter solstice at an angle $\alpha = 42°$, while for the summer solstice, the length ratio presents a lower maximum value at an angle $\alpha = 13°$.

On the other hand, with the aid of **Eq. (7)** the geometrical analysis of the length relationship L_D/l_D is

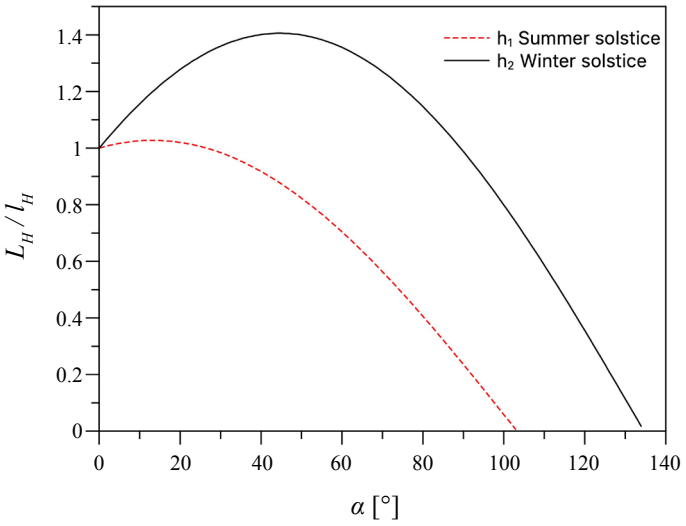

Figure A1. Shading length ratio L_H/l_H versus angle α.

depicted in **Figure A2**, this ratio is shown by varying the angles α and β for different values of the aspect ratio l_H / l_D for the solar heights mentioned above. An increase in the ratio l_H / l_D defines different optimal values of the inclination angles α and β for which the maximum values of L_D / l_D are presented. The shading device aims to provide the longest shading length in summer and winter to avoid thermal gains due to solar exposure.

For greater aspect ratio values up to $l_H / l_D \geq 22$, the angle α presents constant values of $\alpha = 133°$ and $\alpha = 164°$, for the summer and winter solstices, respectively. The value of the angle β, remains invariant with a value $\beta = 90°$. For a length ratio value $l_H / l_D \approx 22$, $\beta = 90°$, the angle value α takes a constant value, as shown in **Table 4**. To analyze the influence of the length ratio on the shading effect, l_H / l_D values of 0.5, 1 and 2 were used.

Table A1. Optimal angles of the shading device for the maximum shading length on roofs.

l_H / l_D	α_{sumeer} [°]	α_{winter} [°]	β
0.5	72	103	90
0.75	82	114	90
1	90	122	90
2	109	140	90
⋮	⋮	⋮	⋮
22	133	164	90
23	133	164	90
24	133	164	90

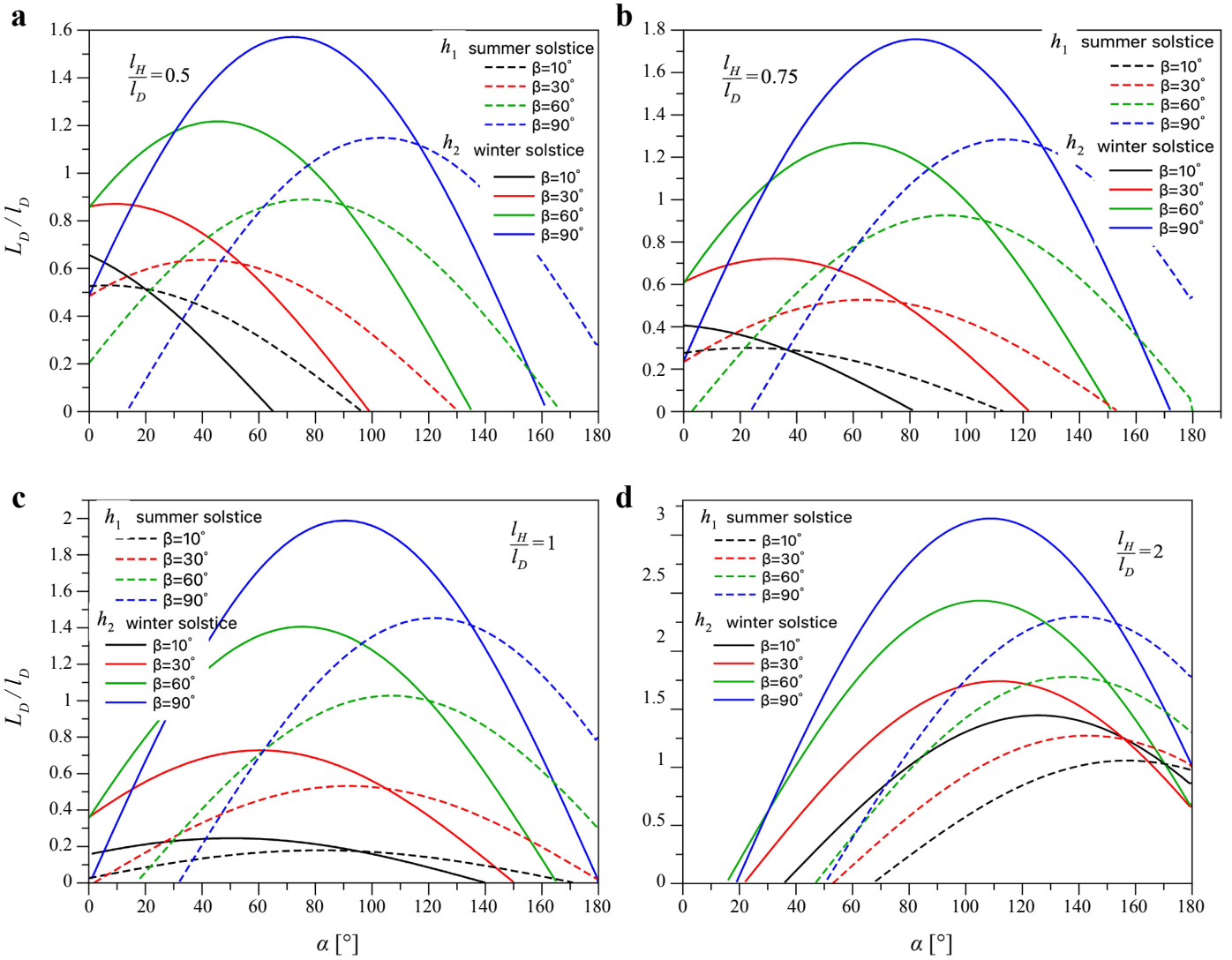

Figure A2. Shading length ratio L_D / l_D versus plate angles α and β, for **a)** $l_h / l_D = 0.5$, **b)** $l_h / l_D = 0.75$, **c)** $l_h / l_D = 1$ and **d)** $l_h / l_D = 2$.